Influence of the Laser Prepulse on Proton Acceleration in Thin-Foil Experiments

M. Kaluza, J. Schreiber, M. I. K. Santala, G. D. Tsakiris, K. Eidmann, J. Meyer-ter-Vehn, and K. J. Witte

Max-Planck-Institut für Quantenoptik, Hans-Kopfermann-Straße 1, D-85748 Garching, Germany

(Received 8 December 2003; published 20 July 2004)

We investigate the influence of the laser prepulse due to amplified spontaneous emission on the acceleration of protons in thin-foil experiments. We show that changing the prepulse duration has a profound effect on the maximum proton energy. We find an optimal value for the target thickness, which strongly depends on the prepulse duration. At this optimal thickness, the rear side acceleration process leads to the highest proton energies, while this mechanism is rendered ineffective for thinner targets due to a prepulse-induced plasma formation at the rear side. In this case, the protons are primarily accelerated by the front side mechanism leading to lower cutoff energies.

DOI: 10.1103/PhysRevLett.93.045003 PACS numbers: 52.38.Kd, 29.30.Ep, 41.75.Jv

Proton and ion acceleration using high-intensity lasers is a field of rapidly growing interest. For possible applications of proton beams produced in laser-solid interactions like the imaging of electromagnetic fields in overdense plasmas [1] and the envisaged usage of proton beams in the fast-ignitor scenario [2], the generation of beams with controllable parameters such as energy spectrum, brightness, and spatial profile is crucial. Hence, for the reliable generation of proton beams, the physics underlying the acceleration processes has to be well understood. After the first proof-of-principle experiments [3–6], systematical studies were carried out to examine the influence of target material and thickness [7–9]. To establish the influence of the main laser parameters such as intensity, pulse energy, and duration over a wide range, results from different laser systems have to be compared, since usually each system covers a small parameter range only. Besides these parameters, strength and duration of the prepulse due to amplified spontaneous emission (ASE) play an important role, too [7], but until now a detailed investigation has not yet been carried out.

In most experiments, protons with energies exceeding 1 MeV have been observed. They originate from water and hydrocarbon molecules adsorbed at the target surfaces due to the unavoidable presence of water and pump oil vapor in the target chamber. The origin of the most energetic protons is still debated. There are at least two acceleration scenarios able to explain the occurrence of MeV protons. (i) They may come from the *front* surface of the target, i.e., the side irradiated by the laser pulse [3,4,10] or (ii) from the *rear* surface [5,11,12]. Recent results indicate that both mechanisms act simultaneously [13,14], in accordance with the predictions of multidimensional particle-in-cell (PIC) codes [15,16].

In this Letter, we report on experiments performed to investigate the effect both of the ASE prepulse duration and the target thickness on the acceleration of protons. The proton cutoff energy depends very sensitively on the combination of these two parameters. For a fixed prepulse duration, the highest proton energies are obtained at an optimal target thickness, which in turn is determined by the ASE prepulse duration. The results can be consistently interpreted if one assumes that above this thickness, the fastest protons are accelerated at the target rear side, while for thinner targets this mechanism is rendered ineffective and only the front side acceleration is active, resulting in lower proton cutoff energies. Furthermore, our results allow a comparison of the experimental results obtained with different laser systems.

The experiments were carried out with the ATLAS laser system at the Max-Planck-Institut für Quantenoptik. It consists of a MIRA oscillator delivering 100-fs pulses of 790-nm wavelength. The pulses are stretched to 160 ps followed by a regenerative amplifier (RA), two multipass amplifiers, and a grating compressor. The output pulses have a duration of $\tau_L = 150$ fs (FWHM) with an on-target energy, E_L, between 600 and 850 mJ. The p-polarized beam is focused under 30° incident angle by a $f/2.5$ off-axis parabolic mirror onto Al foils of 0.75 to 86-μm thickness. About 60% of the pulse energy is contained in a spot of $r_f \approx 2.5$ μm radius, resulting in an averaged intensity, I_L, slightly above $10^{19}\,\mathrm{W/cm^2}$ within this spot. The high-intensity part of the pulse is preceded by a 6-ns long low-intensity pedestal due to ASE mainly generated in the RA. The prepulse duration can be controlled by means of an ultrafast Pockels cell located after the RA with a top-hat-like temporal gate of 6-ns duration. The rise time of the leading edge is 300 ps and the gate jitter is 150 ps. By changing the position of the gate relative to the main pulse, the pedestal is either fully or partially transmitted or almost fully suppressed to a minimum prepulse duration of (500 ± 150) ps. The intensity ratio between main and prepulse is better than 2×10^7 and the increase of the intensity above the pedestal level, as measured by a third-order autocorrelator [17], starts 11 ps before the peak intensity.

Two different proton detectors were used. Pieces of CR 39 were placed 82 mm behind the target to record the spatial profile of the proton beam. Covering a half-opening angle of ~20°, they were wrapped with a 12-μm

Al foil to filter out heavier ions and protons with energies below 900 keV. Through a small hole around the target normal direction, ions could pass to be detected by a Thomson parabola. In such a spectrometer, ions with different charge-to-mass ratios are dispersed by parallel electric and magnetic fields onto distinct parabola tracks in the plane of the detector (CR 39). After etching the CR 39, the ion pits were counted under a computer-controlled microscope, revealing the exact energy spectra.

We have performed several series of measurements, varying the ASE duration, τ_{ASE}, the laser intensity, I_L, and the target thickness. Figure 1 shows the measured proton cutoff energies versus the target thickness for $I_L = 1.0 \times 10^{19}\,\mathrm{W/cm^2}$ and ASE durations of 0.5, 0.7, and 2.5 ns, respectively. For each duration we find that with increasing target thickness the cutoff energy first increases and then drops again. The highest proton energies are achieved at an optimal target thickness. When the prepulse duration is changed, this optimal value changes correspondingly, as it is shown in the inset. For thicker targets, the prepulse duration appears to have no effect on the proton cutoff energies, whereas for thinner targets and longer τ_{ASE} the cutoff energies are reduced.

To check the influence of the laser intensity, we have performed shots with constant prepulse duration of 2.5 ns but slightly different laser intensities by changing the laser energy (Fig. 2). While the proton cutoff energies strongly depend on I_L, the optimal thickness appears to depend on the prepulse duration only (cf. Fig. 1).

The proton spectra around the optimal target thickness measured with an intensity of $1.3 \times 10^{19}\,\mathrm{W/cm^2}$ and a prepulse duration of 2.5 ns are plotted in Fig. 3. In addition to the rather cold proton component dominating the spectrum of the 2-μm foil with a Boltzmann-like temperature of 250 ± 30 keV, a population with a significantly higher temperature of 800 ± 200 keV and 4.0 ± 0.6 MeV appears in the 5 and 8.5-μm foil spectra, respectively. The temperatures of the hottest proton component, given in the inset, exhibit a similar behavior as the cutoff energies, i.e., the proton temperature drastically decreases below the optimal target thickness.

The spatial profiles of the proton beam also change around the optimal thickness. Figures 4(a)–4(c) show the proton beam profiles obtained with targets 2, 5, and 8.5 μm thick. While the first profile is rather blurred, a collimated feature aligned along the target normal appears in Figs. 4(b) and 4(c), persisting for all thicker targets.

The significant changes in proton spectra and beam profiles described above can be interpreted as a transition between two regimes delimited by the optimal thickness: (i) Only the front side acceleration is active for targets thinner than the optimal thickness and (ii) protons are accelerated from both target surfaces for target thicknesses above the optimal value. In this second regime, the rear side acceleration leads to higher cutoff energies. This mechanism is suppressed in the first regime due to the formation of an ASE-induced density gradient at the rear side of the target.

On the target front side, the high-intensity part of the laser pulse interacts with a plasma created by the ASE prepulse. Electrons are expelled from high-intensity regions by the ponderomotive potential of the laser, $\varphi_p = m_e c^2(\gamma_{\mathrm{os}} - 1)$, until it is balanced by the electrostatic potential arising from the charge separation. Here, $\gamma_{\mathrm{os}} = \sqrt{1 + I_L \lambda_L^2/(1.37 \times 10^{18}\,\mathrm{W\,cm^{-2}}\,\mu\mathrm{m}^2)}$ is the relativistic factor, m_e the rest mass of the plasma electrons. Sentoku *et al.* showed [18] that protons can initially gain kinetic energies approaching this potential, when the laser pulse

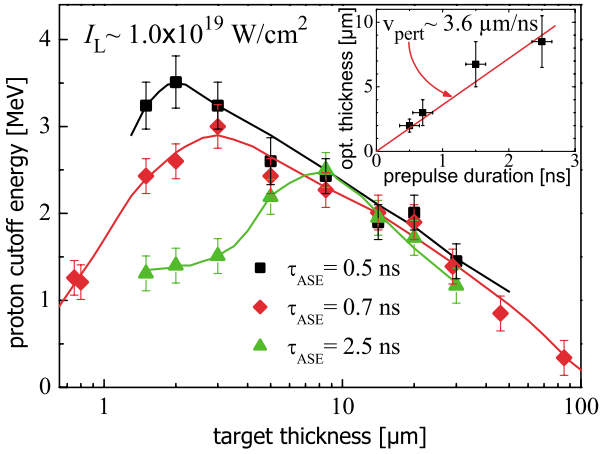

FIG. 1 (color). Proton cutoff energies for differently thick targets and prepulse durations, τ_{ASE}, of 0.5, 0.7, and 2.5 ns, respectively, at $I_L = 1.0 \times 10^{19}\,\mathrm{W/cm^2}$. For longer τ_{ASE}, the maximum proton energies are achieved with thicker foils. The inset gives the optimal thickness, depending on τ_{ASE}.

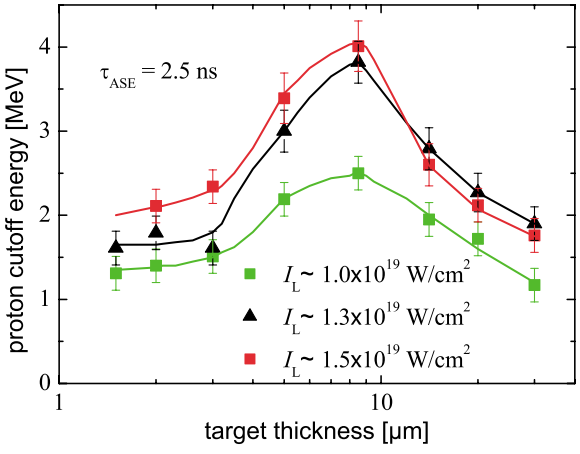

FIG. 2 (color). Proton cutoff energies for differently thick targets and different laser intensities for a prepulse duration of $\tau_{\mathrm{ASE}} = 2.5$ ns. The cutoff energies vary with the laser intensity, but the optimal target thickness depends on τ_{ASE} only (cf. Fig. 1).

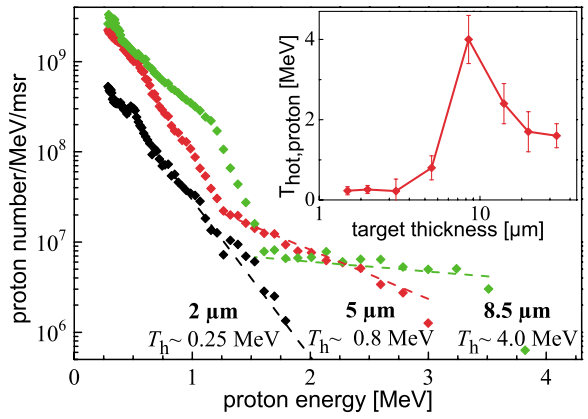

FIG. 3 (color). Proton spectra at $I_L = 1.3 \times 10^{19}$ W/cm^2 for $\tau_{\mathrm{ASE}} = 2.5$ ns and 2, 5, and 8.5 μm thick foils. With increasing target thickness, a second hotter proton population with much higher cutoff energies appears. The inset gives the temperatures of the hot proton component for all measured thicknesses. A similar behavior is observed for all different τ_{ASE}.

is longer than the acceleration time $\tau_a = \lambda_L/c \times \sqrt{m_p/m_e\gamma_{\mathrm{os}}}$, where m_p is the proton mass. For our conditions, we have $\tau_a = 70$ fs, which is shorter than our pulse duration, and φ_p varies between 0.72 and 0.92 MeV, depending on I_L. During the acceleration, a sharp proton front is formed, that expands afterwards due to an electrostatic repulsion within this front, additionally increasing the peak proton velocity by 50% [18], and thus resulting in cutoff energies of $1.5^2 \times \varphi_p \approx 1.6 \ldots 2.1$ MeV for protons accelerated at the front side of the target.

The target normal sheath acceleration (TNSA) mechanism is responsible for proton acceleration from the target rear side [15]. At the front side, a fraction of $\eta \approx 25\%$ of the laser energy is converted into fast electrons having a mean energy of $k_B T_e \approx m_e c^2(\gamma_{\mathrm{os}} - 1)$ [19], resulting in a total number $N_e \approx \eta E_L/k_B T_e$ of hot electrons that propagate through the target. Arriving at the rear side, only a small fraction of the fastest electrons can escape, while the target charges up. Most of the electrons are held back

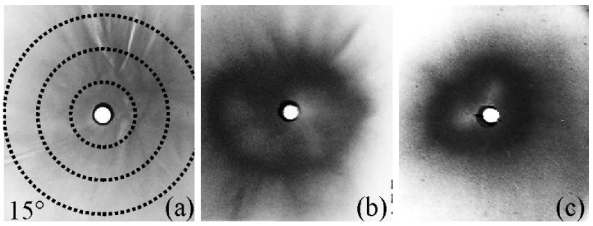

FIG. 4. Proton beam profiles for $\tau_{\mathrm{ASE}} = 2.5$ ns recorded on CR 39 for 2, 5, and 8.5 μm thick targets, respectively. While in (a) the profile is blurred, we observe in (b) and (c) that the major part of the beam is well collimated along the target normal direction. This collimated feature appears only for targets at and above the optimal thickness. The circles in (a) give half-opening angles of 5°, 10°, and 15°, respectively.

by the arising electic field and form a sheath at the rear side with a Debye length of $\lambda_D = \sqrt{\varepsilon_0 k_B T_e/n_e e^2}$. This field ionizes atoms at the rear surface and accelerates them in target normal direction. Mora described the acceleration process with 1D simulations [20]. Here, the target consists of preionized hydrogen. The electrons, having a mean energy of $k_B T_e$ during the laser pulse duration, are assumed to be in thermal equilibrium with the electrostatic potential Φ at the target rear side, i.e., $n_e = n_{e0} \times \exp(e\Phi/k_B T_e)$. On the other hand, Φ can be obtained from the Poisson equation $\varepsilon_0 \partial^2\Phi/\partial x^2 = e(n_e - n_p)$, taking into account the electron and proton densities. Initially, the proton density, n_p, is steplike with $n_p = n_{e0}$ in the target. By iteratively solving the equation of motion and the continuity equation for the protons, their new density in the next time step is obtained, leading to a new potential and electric field. As the field is always peaked at the proton front, the fastest protons are also located there. Mora also found an analytical expression for the evolution of the maximum proton energy, E_p, as a function of the interaction time, t_i, depending only on the electron temperature, T_e, and the initial electron density, n_{e0}:

$$E_p \approx 2k_B T_e \left\{ \ln\left[\frac{t_i \omega_{pp}}{\sqrt{2e_E}} + \sqrt{1 + \left(\frac{t_i \omega_{pp}}{\sqrt{2e_E}} \right)^2} \right] \right\}^2. \quad (1)$$

$\omega_{pp} = \sqrt{n_{e0} e^2/\varepsilon_0 m_p}$ is the proton plasma frequency, that depends on n_{e0}, and $e_E = 2.71828\ldots$. We assume $t_i \approx \tau_L$, the same electron numbers and temperatures on both target surfaces, and a constant divergence of the electron beam propagating through the target. The hot electron density at the rear side, n_{e0}, is estimated as follows. Accelerated in the laser focus with an initial radius of $r_f = 2.5$ μm and a half-opening angle of θ_{in}, the electron beam travels through an effective target thickness of $d_t^* = d_t/\cos 30°$ and leaves it within an area of $\pi(r_f + d_t^* \tan\theta_{\mathrm{in}})^2$. Assuming an electron bunch length of $c\tau_L$, the averaged electron density at the rear side is

$$n_{e0} \approx \frac{N_e}{c\tau_L \times \pi(r_f + d_t^* \tan\theta_{\mathrm{in}})^2}. \quad (2)$$

The peak proton energies for differently thick targets calculated with Eqs. (1) and (2) are compared in Fig. 5 with the experimental results for $I_L = 1.3 \times 10^{19}$ W/cm^2 and $\tau_{\mathrm{ASE}} = 2.5$ ns. The cutoff energies for targets optimally thick and thicker are well described by this model for an initial half-opening angle of $\theta_{\mathrm{in}} = (8 \pm 2)°$, which is comparable to the value found in [21]. For the same θ_{in}, this model describes also well the results from Fig. 1, when the reduced laser intensity is taken into account.

The cutoff energies for thinner targets cannot be explained by the TNSA mechanism assuming a steplike density gradient at the rear side. Because of the ASE prepulse, a plasma is formed at the target rear surface,

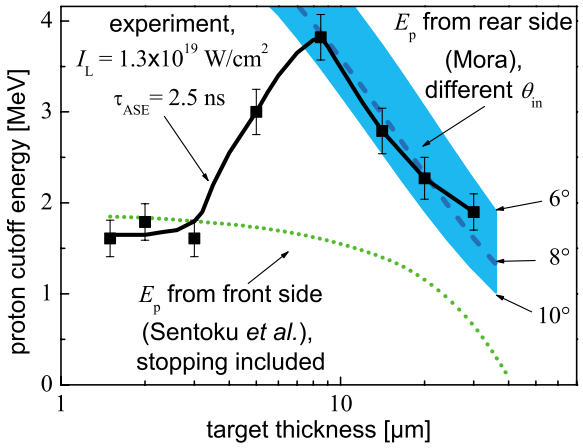

FIG. 5 (color). Comparison of experimental data for $\tau_{ASE} = 2.5$ ns and $I_L = 1.3 \times 10^{19}$ W/cm^2 with theoretical predictions. The dotted line gives the cutoff energy for front side accelerated protons including their stopping in the target, while the broad area gives the maximum rear side proton energies for a range of opening angles $\theta_{in} = (8 \pm 2)°$ of the electron beam.

reducing the acceleration fields [12,19]. We investigated the evolution of this rear side density gradient using the 1D-hydro code MULTI-FS [22]. A simulation for the rear side proton acceleration as described above, that starts with the same rear side density gradient as predicted by MULTI-FS, gives much lower proton cutoff energies for the thinnest foils than those observed in the experiment. Therefore, the rear side acceleration process alone is not able to explain the measured proton energies for all foil thicknesses. On the other hand, protons accelerated at the target front side are not affected by a plasma at the rear side [12]. The maximum energy for front side protons predicted by Sentoku *et al.* [18] reproduces the experimental data much better. Their initial energy is determined by the laser intensity only. The comparison with this model including proton stopping in the target [23] is shown in Fig. 5, yielding a good agreement for the thinnest foils. The increase of the proton cutoff energy for thin targets due to electron recirculation in the target [8] could not be observed, because in our experiment the laser contrast ratio was 500 times lower.

The optimal target thickness is found to depend on the ASE duration only (cf. Figs. 1 and 2). This dependency can be approximated linearly with a slope of $v_{pert} \approx 3.6\,\mu$m/ns (cf. Fig. 1). MULTI-FS simulations show that (i) the prepulse launches a shock wave into the target and (ii), the bulk of the target is radiatively heated due to x rays generated in the focus of the prepulse on the target front side. Both effects can cause an expansion of the target. While the shock wave is weak for our prepulse conditions, the radiative heating is sufficiently strong to form a rear side density gradient for the thinnest foils. In contrast, due to the absorption of radiation in the bulk of the target, the formation of a rear side density gradient sets in at later times for thicker targets. The onset of this plasma formation as observed in MULTI-FS simulations defines the optimal thickness for proton acceleration. The simulation results reproduce the experimentally found value of $3.6\,\mu$m/ns. Although slightly dependent on the ASE intensity, which could not be varied during the experiment, this value can be used to estimate the effect of the prepulse in various laser systems, each having a fixed prepulse duration, on the rear side ion acceleration [9].

In conclusion, we demonstrated a strong influence of the ASE prepulse on the laser-initiated acceleration of protons. An optimal target thickness for the proton acceleration was found. This optimal value depends linearly on the ASE duration and it is determined by a prepulse-induced formation of an ion-density gradient at the rear side of the target. Furthermore, we were able to distinguish between the two main proton acceleration mechanisms, the fastest protons are accelerated from the rear side of the target having the optimal thickness. Analytical estimates support this interpretation. The determination of the optimal target thickness allows a better comparison between existing experimental results and can help to optimize the conditions for proton acceleration for a large range of laser systems in the future.

We thank S. Karsch and P. Mora for fruitful discussions and H. Haas and A. Böswald for the technical support. This work was supported by Euratom-IPP and the EU project SHARP (Contract No. HPRI-CT-2001-50012).

[1] M. Borghesi *et al.*, Phys. Rev. Lett. **88**, 135002 (2002).
[2] M. Roth *et al.*, Phys. Rev. Lett. **86**, 436 (2001).
[3] A. Maksimchuk *et al.*, Phys. Rev. Lett. **84**, 4108 (2000).
[4] E. Clark *et al.*, Phys. Rev. Lett. **84**, 670 (2000).
[5] R. Snavely *et al.*, Phys. Rev. Lett. **85**, 2945 (2000).
[6] S. Hatchett *et al.*, Phys. Plasmas **7**, 2076 (2000).
[7] M. Roth *et al.*, Phys. Rev. ST Accel. Beams **5**, 061301 (2002).
[8] A. Mackinnon *et al.*, Phys. Rev. Lett. **88**, 215006 (2002).
[9] I. Spencer *et al.*, Phys. Rev. E **67**, 046402 (2003).
[10] E. Clark *et al.*, Phys. Rev. Lett. **85**, 1654 (2000).
[11] M. Hegelich *et al.*, Phys. Rev. Lett. **89**, 085002 (2002).
[12] A. Mackinnon *et al.*, Phys. Rev. Lett. **86**, 1769 (2001).
[13] S. Karsch *et al.*, Phys. Rev. Lett. **91**, 015001 (2003).
[14] M. Zepf *et al.*, Phys. Rev. Lett. **90**, 064801 (2003).
[15] S. Wilks *et al.*, Phys. Plasmas **8**, 542 (2001).
[16] A. Pukhov, Phys. Rev. Lett. **86**, 3562 (2001).
[17] S. Karsch, Ph.D. thesis [MPQ-Report 279 (2003)].
[18] Y. Sentoku *et al.*, Phys. Plasmas **10**, 2009 (2003).
[19] S. Wilks *et al.*, Phys. Rev. Lett. **69**, 1383 (1992).
[20] P. Mora, Phys. Rev. Lett. **90**, 185002 (2003).
[21] J. Santos *et al.*, Phys. Rev. Lett. **89**, 025001 (2002).
[22] K. Eidmann *et al.*, Phys. Rev. E **62**, 1202 (2000).
[23] http://physics.nist.gov/